Conducting Pathways in Organic Solids: A Phenalenyl-Based Neutral Radical of Low Conductivity†

X. Chi,‡ M. E. Itkis,‡ R. W. Reed,§ R. T. Oakley,§ A. W. Cordes,|| and R. C. Haddon*,‡

Departments of Chemistry and Chemical & Environmental Engineering, University of California, Riverside, California 92521-0403, Department of Chemistry, University of Waterloo, Waterloo, Ontario N2L 3G1, Canada, and Department of Chemistry and Biochemistry, University of Arkansas, Fayetteville, Arkansas 72701

Received: March 22, 2002; In Final Form: June 6, 2002

The passage of a current through a solid requires a pathway for the movement of electrons or holes. A new class of phenalenyl-based neutral radical molecular conductors has recently been reported; a distinctive feature of these molecular solids is the absence of any obvious conducting pathway(s). These radicals do not stack in the solid state, and the requisite carbon−carbon contacts are all larger than the sum of the van der Waals distances. Magnetic susceptibility measurements show that the first compound to be isolated behaves as a free radical with one spin per molecule, apparently supporting the idea that there is little interaction between the molecules in the solid state. Nevertheless, this radical shows the highest conductivity ($\sigma_{RT} = 0.05$ S/cm), of any neutral organic solid, and the conduction mechanism is presently unresolved. In the present study, we report a structurally related radical with a resistivity 4 orders of magnitude higher than that of the previously reported radicals. We analyze the crystallographic and electronic structure of these solids in detail and argue that a conducting pathway is operative in many of these neutral radicals. We show that the very weak orbital overlap between well-spaced neighbors is sufficient to provide a conducting pathway in carbon-based free radicals providing that the π-systems are not perpendicular, and we further argue that such effects may be operative in other organic molecules.

Introduction

It is fundamental to our understanding of transport processes in solid-state materials that conductivity comes about as result of a conducting pathway and the availability of carriers (electrons or holes). In almost all cases, and particularly for organic materials, the identification of the conducting pathway is readily discerned in terms of orbital overlap. That is, by an examination of the localized states associated with the charge carriers, the orbital overlap that is responsible for the conducting pathway through the solid is readily identified. In fact, this has been one of the most useful tools in designing organic conducting solids, and there is a large amount of literature that is devoted to this principle. It is important to note that this understanding of the relationship between conductivity and orbital overlap is not necessarily based on sophisticated theories of electronic structure, but is usually made obvious in the simplest methods, such as the Extended Huckel Theory (EHT).[22] It is for this reason that EHT band structure calculations have been widely used in the rationalization of the electronic structure of organic conductors and superconductors.[35]

In many highly conducting charge-transfer salts, such as TTF-TCNQ (tetrathiafulvalene-tetracyanoquinodimethane)[36,10,8] and $(TMTSF)_2ClO_4$ (tetramethyl-tetraselenafulvalene-perchlorate),[3,2] the electron-donors stack to form one-dimensional (1D) or pseudo-1-D structures (Figure 1).[28,26,2] The $\pi-\pi$ interaction

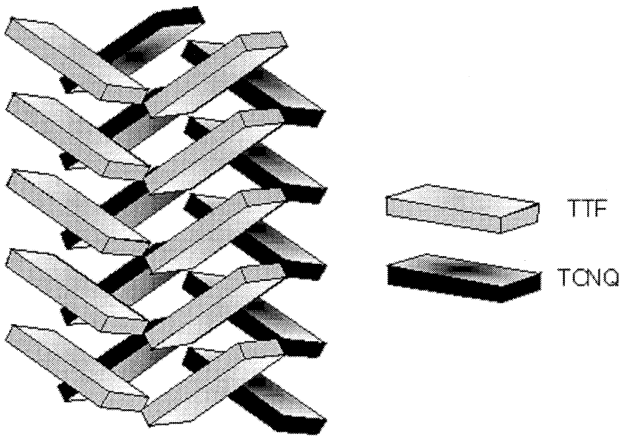

Figure 1. Diagram showing 1-D stacking of the planar molecules in the TTF-TCNQ charge-transfer salt.[28,26]

along the stacking direction provides an effective and obvious conducting pathway in these solids. Most of the ethylenedithiotetrathiafulvalene (ET)-based superconductors[27,37] crystallize as 2-D layered structures. Although stacking of the donor molecules is found in some ET salts (α- and β-$(ET)_2I_3$),[24,4,34] there are no stacks in κ-$(ET)_2Cu(NCS)_2$ [33,5] ($T_c = 10.4$ K) and other κ-phase ET-based superconductors,[25] and it is generally believed that the sulfur−sulfur intermolecular interactions dominate the transport properties (Figure 2).[5,25,35,38,20]

Organic conductors based solely on carbon atoms are rare, and the C_{60}-based superconductors are special examples. Because C_{60} consists of a sphere of π-orbitals radiating in all directions,[15,20] the π orbitals of the C_{60} molecule overlap in three

† Part of the special Issue "John C. Tully Festschrift".

* To whom correspondence should be addressed.
‡ Departments of Chemistry and Chemical & Environmental Engineering, University of California, Riverside.
§ Department of Chemistry, University of Waterloo.
|| Department of Chemistry and Biochemistry, University of Arkansas.

10.1021/jp020792e CCC: $22.00
Published on Web 07/31/2002

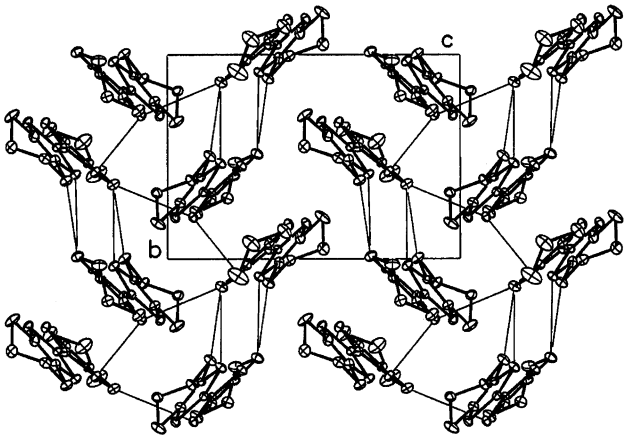

Figure 2. ET donor molecule layer in κ-$(ET)_2Cu(NCS)2$ at 118 K. S··S contacts shorter than 3.6 Å are indicated by thin lines.[5]

dimensions, and these materials exhibit the highest transition temperatures among molecular superconductors.[35]

We reported the first phenalenyl-based neutral radical molecular conductor (**4**), and more recently, a class of dimeric phenalenyl-based neutral radical molecular conductors (**1**, **3**).[7,6] A distinctive feature of these molecular solids is the absence of any obvious conducting pathway(s). These radicals do not stack in the solid state, and the intermolecular (inter-dimer in the case of **1** and **3**) carbon−carbon contacts are all larger than the sum of the van der Waals distances. Magnetic susceptibility measurements show that compound **4** behaves as a free radical with one spin per molecule,[7] indicating that there is little interaction between the molecules in the solid state. Nevertheless, this radical shows the highest conductivity (σ_{RT} = 0.05 S/cm), of any neutral organic solid, and the conduction mechanism is presently unresolved.

We have now crystallized compound **2**, another radical in the family of spiro-bis(1,9-disubstituted phenalenyl)boron compounds, which differs only in the length of the alkyl chain from previous members in the series (**1**, **3**, **4**). Below, we show that the conductivity of radical **2** is 4 orders of magnitude smaller than that of the previously reported radicals, even though the solid-state electronic structure is very similar to that of **4** and particularly **1** (room-temperature paramagnetic π-dimers). This observation suggests that the packing of the molecules in the lattice is of vital importance to the transport properties, and that there must be effective conducting pathways in crystals of radicals **1**, **3**, and **4**, that are absent in crystals of **2**.

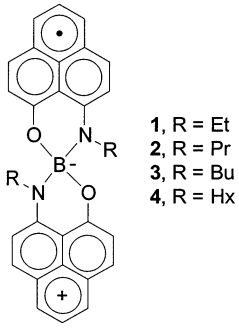

1, R = Et
2, R = Pr
3, R = Bu
4, R = Hx

In the present manuscript, we report the synthesis, crystallization and solid-state properties of radical **2**, and by a careful examination of the packing of the radicals, we attempt to delineate the conducting pathways in these solids. We begin by locating likely conducting pathways in these solids by identifying the closest approaches between pairs of molecules.

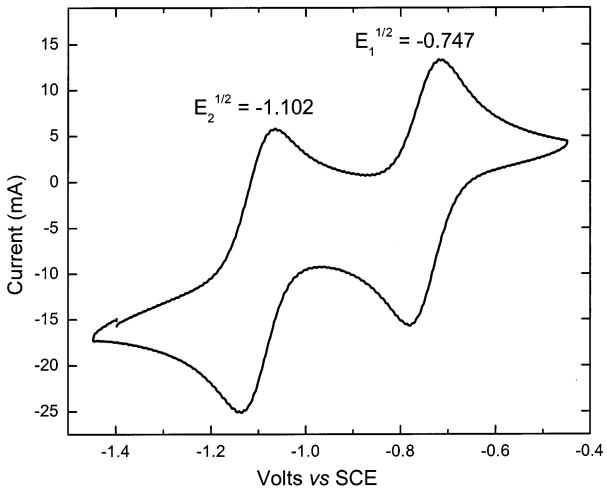

Figure 3. Cyclic voltammetry of **2** in acetonitrile, referenced to SCE via internal ferrocene (not shown).

Next, we assess the strength of the interaction between the pairs of molecules in the lattice by using Extended Huckel Theory (EHT), to calculate the energy splitting between the singly occupied molecular orbitals (SOMOs) of the two molecules involved in the candidate conducting pathways in these solids. We show that the strength of the interaction between neighboring planar π-conjugated carbon-based molecules in the solid state is largely determined by the manner in which two molecules are oriented and arranged. When one molecule lies directly above the plane of the other, the interaction between them is strongest if the planes are parallel to each other (a π-dimer); the interaction is weakened as the angle between the planes increases. This behavior may be attributed to the nodal properties of the pπ-orbitals that contain the spin density in the phenalenyl ring system.

In the case of propyl radical (**2**), the unit cell contains only 2 monomer units (a single π-dimer), whereas the other radicals, contain 4 (two π-dimers; **1** and **3**) or 8 (**4**) monomers in the unit cell. In **2**, (apart from the π-dimers), most phenalenyl units pack perpendicular to each other; where the phenalenyl units are parallel to each other they are in a side-by-side arrangement (without overlap of the molecular planes). Given the fact that the SOMO is composed exclusively of planar π-conjugated carbon atoms, the overlap of these orbitals is ineffective, regardless of the intermolecular spacings. Thus, there are no effective conducting pathways in crystals of propyl radical (**2**), and the conductivity is much lower than that of the other radicals. In crystals of hexyl radical (**4**), however, some phenalenyl units that are directly above each other are not perpendicular; these phenalenyl units have angles of 75−80° between them. We show that this small difference in the relative orientations of these molecular pairs in the two classes of radicals is the main factor in the large difference in the transport properties of the two compounds.

Results

Preparation and Solution Properties of Propyl Radical (2). The synthesis of radical **2** followed the same basic procedures that was used to prepare radicals **1**, **3**, and **4**.[7,6] Because the solubility of $\mathbf{2}^+$, BPh_4^- was very low in organic solvents, we chose tetrakis[3,5-bis(trifluoromethyl)phenyl]borate ($TFPB^-$) as the counterion and thus salt $\mathbf{2}^+$, $TFPB^-$ was used as the precursor to radical **2**. The cyclic voltammetry of salt $\mathbf{2}^+$, $TFPB^-$ (Figure 3) shows two reversible reduction waves,

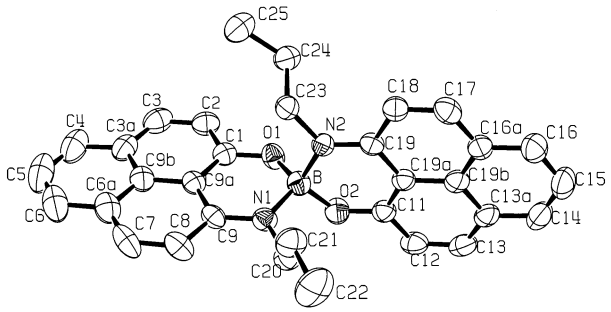

Figure 4. ORTEP drawing of the solid-state structure of the propyl radical (**2**), showing the atom numbering.

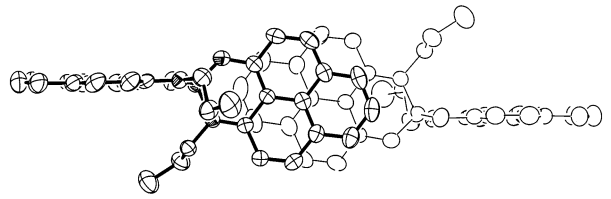

Figure 5. Overlap between one pair of enantiomers of crystalline propyl radical (**2**). In all other Figures we omit the alkyl groups for clarity.

TABLE 1: Crystal Data for Propyl Radical (2)

formula	$BO_2N_2C_{32}H_{28}$
fw	483.39
a, Å	9.450(3)
b, Å	10.230(4)
c, Å	13.600(4)
α, deg	99.670(3)
β, deg	96.540(2)
γ, deg	104.520(3)
V, Å^3	1237.8(7)
space group	$P\bar{1}$
Z	2
T, K	293
μ, mm^{-1}	0.07
refine data (all)	4158
parameters refined	335
$R(F)$, $R_w(F)^a$	0.087, 0.085
$R(F)(F2 > 3\sigma)$	0.043
mean plane separation (Å)	3.400

with a small electrochemical disproportionation energy, $\Delta E_{2-1} = E_2^{1/2} - E_1^{1/2} = -0.36$ V, very similar to the values found for **1**, **3**, and **4**. The ΔE_{2-1} value largely determines the on-site Coulomb correlation energy (U) in the solid state and is well-established as an important discriminator for organic metals;[11,32] the similarity in the values of this parameter among all of the radicals (**1**−**4**), eliminates the properties of the isolated molecules as the origin of the differences in conductivities.

Slow reduction of $\mathbf{2}^+$, $TFPB^-$ by cobaltocene in an H−Cell produces single crystals of propyl radical with sizes much larger ($0.49 \times 0.23 \times 0.13$ mm) than those obtained when $\mathbf{2}^+$, BPh_4^- was used as the precursor.

X-ray Crystal Structure of Propyl Radical (2). Crystals of **2** belong to the triclinic space group $P\bar{1}$, with two radicals per unit cell. Table 1 provides crystal data and Figure 4 shows an ORTEP drawing of the molecule together with the atom numbering.

Radical **2** is chiral and the crystal is composed of pairs of enantiomers. The projection diagram of one pair of enantiomers (Figure 5), illustrates the approximate superposition of the active carbon atoms that carry most of the spin density (1,3,4,6,7,9); this packing arrangement is also observed in crystals of ethyl and butyl radicals (**1** and **3**).[6] The mean plane separation within each π-dimer is 3.4 Å at room temperature, a little longer than that found in the paramagnetic π-dimer of ethyl radical (**2**) (3.35 Å at room temperature).[6] The carbon−carbon contacts between dimers are all larger than the sum of the van der Waals distances and this point will be addressed in the latter part of the paper.

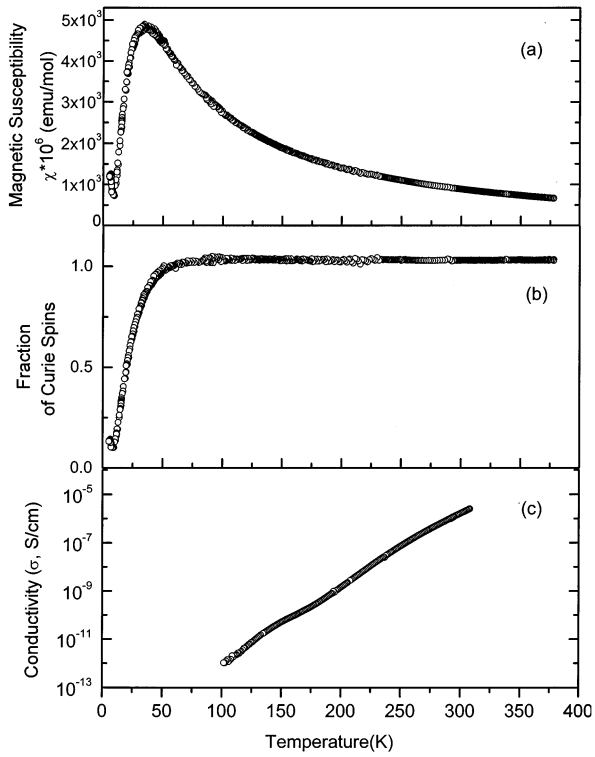

Figure 6. Magnetic susceptibility (a), fraction of Cure spins (b) and single-crystal conductivity (c) of propyl radical (**2**) as a function of temperature.

Magnetic Susceptibility of Propyl Radical (2). Magnetic susceptibility measurements show that radical **2** is paramagnetic (Figure 6a), with one spin per molecule (for temperatures (T) >30 K) (Figure 6b). Thus, within a large temperature range, there exists little evidence for electronic interactions between the molecules and radical **2** appears as a normal isolated organic free radical.

Electrical Conductivity of Propyl Radical (2). The anisotropy in conductivity along the three principal directions of crystals of **2** was measured using a two-probe contact configuration and the measured resistivities along the three crystal directions were found to be comparable at room temperature. The temperature dependence of the electrical resistivity (ρ) was measured on a large single crystal of **2** ($490 \times 225 \times 130$ μm) using four-probe inline contacts along one axis and the results are shown in Figure 6c. The conductivity decreases with decreasing temperature; below 60 K the sample resistance exceeded 10^{13} Ω, the limit of the experimental setup. The room-temperature conductivity (σ) is 1.4×10^{-6} S/cm; 4 orders of magnitude smaller than that of **1**, **3**, and **4** (1.0×10^{-2}, 2.4×10^{-2} and 4.9×10^{-2} S/cm, respectively).

Band Structure of Propyl Radical (2). It should be noted at the outset that there are certain objections to the application of tight binding band theory to the neutral radical molecular conductors,[7] in that the calculations are unable to correctly describe the open shell electronic structure of the materials that prevails in certain temperature regimes for all compounds reported to date, as indicated by the occurrence of Curie paramagnetism.[7,6] A characteristic feature of the previously reported radicals (**1**, **3**, **4**), has been the very narrow bandwidths

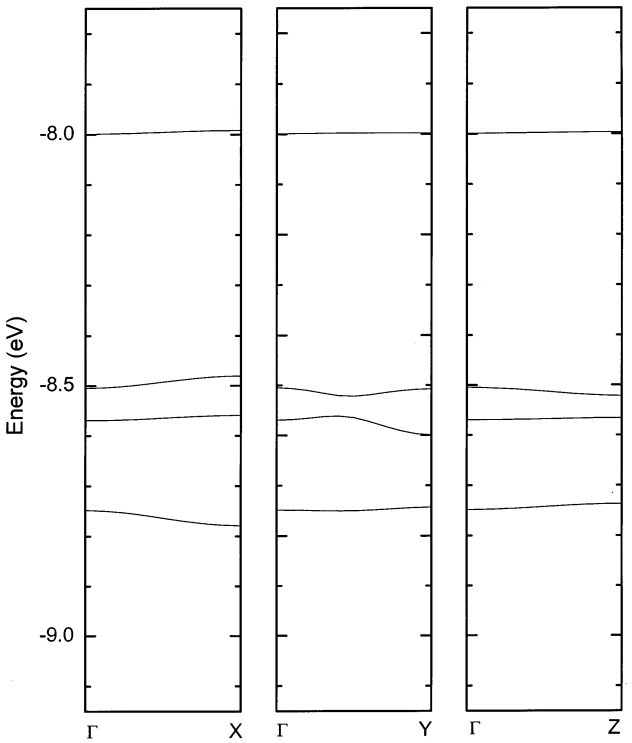

Figure 7. Calculated band structure for crystalline propyl radical (**2**).

found with EHT calculations. The band dispersions found for these compounds are always less than 0.1 eV, whereas most organic metals show EHT bandwidths in the range 0.5−1.0 eV.[35,18,20,29] The small dispersions found for the neutral radical molecular conductors are in accord with expectations based on the large intermolecular spacing found in the crystal structures of **1**, **3**, and **4**.[7,6]

The EHT calculated band structure for **2** is shown in Figure 7; the 4 bands are derived from the two LUMOs of $\mathbf{2}^+$ for each of the 2 molecules of **2** in the unit cell; these basically consist of the symmetric and antisymmetric combinations of the 1,9-disubstituted-phenalenyl LUMO.[17,7] Alternatively, they can be viewed as arising from the nonbonding molecular orbitals[13,14] of each of the 4 phenalenyl units in the unit cell. In a band picture these 4 orbitals now accommodate a total of 2 electrons, leading to a 1/4-filled band complex with 1 filled and 3 vacant bands. The tight binding picture fails of course, because the magnetic susceptibility shows that the electrons are unpaired in compound **2** for $T > 30$ K (Figure 6).

It may be seen that the band dispersion found for **2** is extremely small, even by the standards of **1**, **3** and **4**. The maximum dispersions are 0.036 eV (along a*), 0.075 eV (b*), 0.025 eV (c*) in **4**, with larger values in **1** and **3**;[7,6] the corresponding values in **2** are: 0.030 eV (a*), 0.038 eV (b*), 0.025 eV (c*). Thus, it seems that there is a clear structural difference between **1**, **3**, and **4** and the newly isolated **2** that is captured, at least to some extent, by the EHT band structure calculations. This finding encouraged us to look more closely for differences in the conducting pathways for these compounds, and to use EHT calculations to aid in this examination. The results already support the idea that conductivity in organic solids can be provided by conducting pathways that generate much smaller band dispersions than previously recognized.[18,20]

Conducting Pathways. In the following discussion, we first analyze the packing structures of radicals **2** and **4**. When a continuous interaction between molecules along a certain direction forms a possible conducting pathway, two neighboring molecules in the pathway are selected and Extended Huckel (EHT) calculations are carried out on this pair of molecules to evaluate the strength of the interaction by the energy of the splitting of the SOMOs. This procedure follows previous approaches to the calculation of transfer integrals in organic conductors.[12,23,35] The energy of the dimer splitting is equivalent to twice the transfer integral (t) in the tight-binding approximation. The relative conductivity (σ) in two different directions (a and b), is approximately given by $\sigma_a/\sigma_a = (d_a\, t_a/d_b\, t_b)^2$, where d_a and d_b are the average intermolecular distances.[12,23,35] Thus, within the limitations of EHT theory, the possible conducting pathways along different directions in the crystal lattice can be quantitatively assessed.

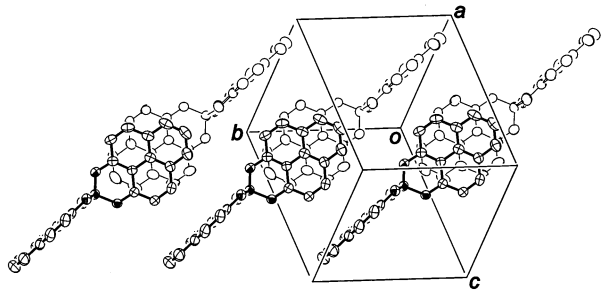

Figure 8. π-Dimer pairs of **2** form columns along the b direction. Three π-dimer pairs are shown, viewed perpendicular to the phenalenyl units involved in dimers.

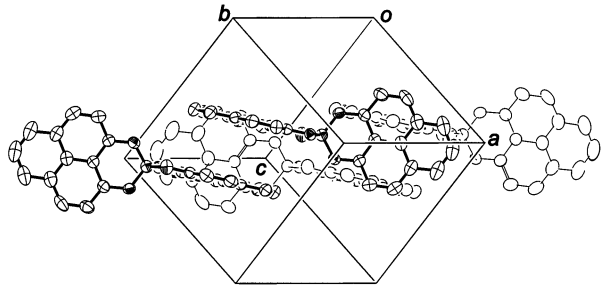

Figure 9. Within a column (along b) the phenalenyl units of neighboring π-dimers are in a perpendicular orientation. Two neighboring π-dimer pairs are shown, viewed perpendicular to the phenalenyl units without $\pi-\pi$ interactions.

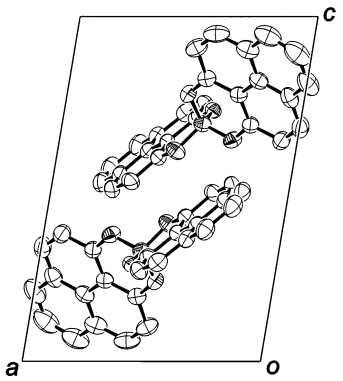

Figure 10. A column of radical **3** shown in Figures 8 and 9 appears as a single π-dimer (projected down b).

Crystal Packing of the Propyl Radical (2). The paramagnetic π-dimer pairs of radical **2** form columns (not stacks) along the b direction of the unit cell (Figure 8). Within each column, the phenalenyl unit that is not involved in a π-dimer interacts exclusively with the phenalenyl unit that is a part of a π-dimer, but in a perpendicular orientation (Figures 8 and 9). When projected down b, each column appears as one pair of π-dimers (Figure 10).

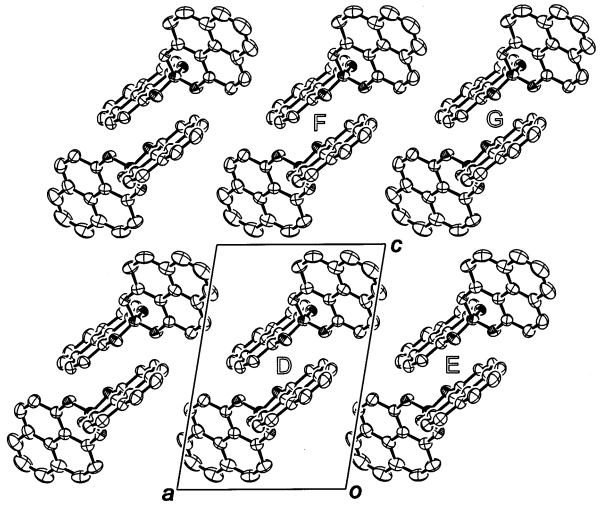

Figure 11. Columns of radical **2** in the crystal. Each π-dimer pair represents a column along *b* (viewing down *b*).

Figure 10 can be extended along the *a* and *c* directions to produce a sheet which can generate the complete lattice when repeated along *b*, as shown in Figure 11. The π-dimer pairs represent columns of **2** down *b*. To form a conducting pathway-(s), the interaction between molecules must be continuous throughout the solid; in other words, the interaction between dimers is more important than that within a dimer in realizing a conducting pathway. Basically, there are two types of possibilities: (1) conducting pathways formed by the interactions between dimers within a column (so that the column shown in Figure 8 forms a possible conducting pathway), (2) conducting pathways formed by the interactions between dimers of different columns. Figure 11 shows 3 possible interactions between dimers from neighboring columns: D and E, D and F, and D and G.

Figure 12 shows three neighboring π-dimer pairs in a column (view down *a*, refer to Figures 8, 9, and 10). It is immediately apparent that there exists two sets of molecules: the molecules shown on the top of Figure 12 form one sub-column of parallel molecules and those on the bottom (enantiomers) form the other sub-column. Therefore, there are two kinds of interactions between dimer pairs: the interaction between molecules belonging to the same sub-column, which is referred to as the interaction in "pathway 1" (the closest carbon−carbon contact is $d1 = 3.678$ Å, Figure 12) and that between molecules belonging to different sub-columns (pathway 2, the closest

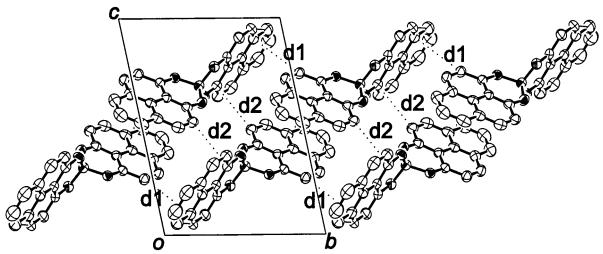

Figure 12. Interactions between molecules within a column. View down *a*, showing the closest contacts of the carbon atoms along the *b* direction.

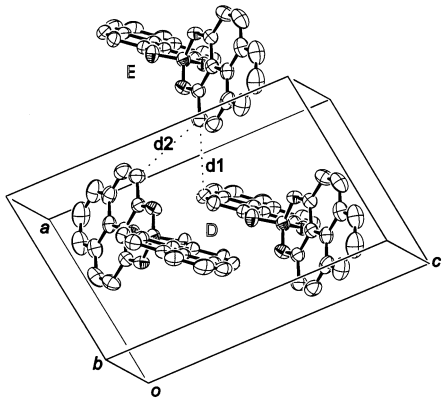

Figure 13. Interactions between the closest molecules in the adjacent columns D and E (see Figure 11).

carbon−carbon contact is $d2 = 3.559$ Å). The calculation shows that the interaction in "pathway 1" is the strongest in crystals of radical **2** (Table 2). This is probably because the phenalenyl units involved in this interaction are directly above each other, whereas the phenalenyl units involved in the interactions in the other pathways are to the side of each other. It is important to note that the phenalenyl units involved in these interactions are all perpendicular to each other (refer to Figures 8 and 9). The consequence of the perpendicular geometry will be discussed later.

Figure 13 illustrates the interactions between the nearest dimer pairs belonging to columns D and E (the other molecule forming the π-dimer pair with the molecule on the top is omitted). The closest carbon−carbon contacts are $d1 = 3.743$ Å and $d2 = 3.778$ Å, and the phenalenyl units involved in these interactions are either perpendicular (d1) or parallel to (and to the side of) each other (d2). Both interactions may form conducting

TABLE 2: Energy of the Singly Occupied Molecular Orbital (SOMO), and the Energy Splitting Caused by a Pair of Molecules in the Lattice of Propyl (2) and Hexyl Radical (4)

compd	constituents	interaction	closest C··C contacts (Å)	energies (eV)		splitting (eV)
propyl radical (**2**)	single molecule			−8.596		
	two molecules	$\pi-\pi$ (dimer pair)	3.4 (Figure 5)	−8.562	−8.765	0.203
	two molecules within a column	pathway 1 (perpendicular)	3.678 (Figure 12)	−8.586	−8.599	0.013
		pathway 2 (perpendicular)	3.559 (Figure 12)	−8.586	−8.587	0.001
	two molecules between columns	pathway 3 (perpendicular)	3.743 (D−E) (Figure 13)	−8.591	−8.596	0.005
		pathway 4 (parallel)	3.778 (D−E) (Figure 13)	−8.594	−8.597	0.002
		pathway 5 (parallel)	3.728 (D−F) (Figure 14)	−8.588	−8.599	0.011
		pathway 6 (parallel)	3.723 (D−G) (Figure 15)	−8.595	−8.596	0.001
hexyl radical (**4**)	single molecule			−8.569		
	two molecules within a column	pathway 1 (perpendicular)	3.488 (J−J) (Figure 17)	−8.562	−8.570	0.008
	two molecules between columns	pathway 2 ($\theta = 80°$)	3.718 (J−K) (Figure 19)	−8.555	−8.573	0.018
		pathway 3 ($\theta = 77°$)	3.688 (L−K) (Figure 21)	−8.556	−8.580	0.024
		pathway 4	3.596 (M−K) (Figure 22)	−8.559	−8.575	0.016
		pathway 5	3.624 (N−L) (Figure 22)	−8.567	−8.568	0.003

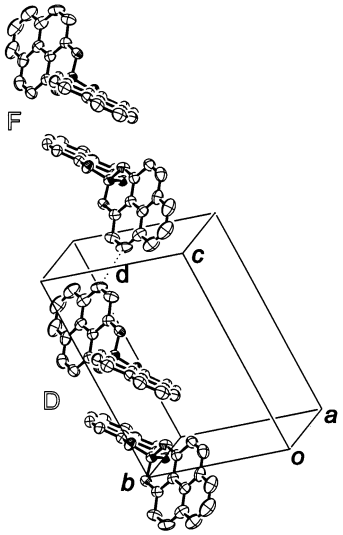

Figure 14. Interactions between the closest molecules in columns D and F (see Figure 11).

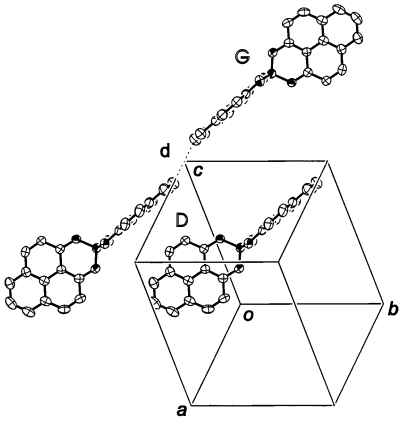

Figure 15. Interactions between the closest molecules in columns D and G (see Figure 11).

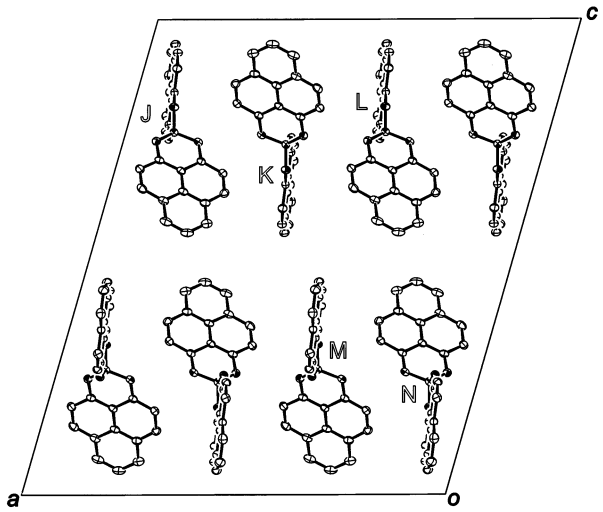

Figure 16. Crystalline **4**, there are eight molecules in the unit cell (viewed down *b*). Each of these molecules forms a column along the *b* direction (Figure 17).

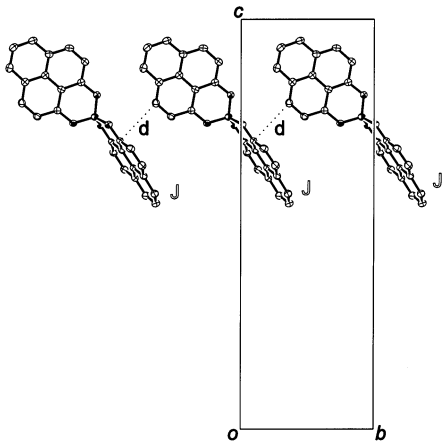

Figure 17. Hexyl radicals (**4**) form columns along the *b* direction (viewed down *a*, only molecule J in Figure 16 is shown here). The interacting phenalenyl units of the neighboring molecules within a column are perpendicular to each other.

pathways, and we refer to them as the interactions for "pathway 3" and "pathway 4", respectively. The calculations (Table 2) show that both interactions are much weaker than those involved in "pathway 1", and the continuous pathways involving these interactions are not considered to play a significant role in the conductivity.

The interactions between nearest dimer pairs from columns D and F (see Figure 11) are illustrated in Figure 14. The closest carbon−carbon contact $d = 3.728$ Å, and the two phenalenyl units are parallel to (but not directly above) each other, and we refer to this interaction as "pathway 5".

The interaction between molecules from columns D and G are illustrated in Figure 15. The closest carbon−carbon contact $d = 3.723$ Å, and the phenalenyl units involved are parallel to each other. The interaction is referred as "pathway 6".

EHT Calculations on Pairs of Molecules in the Lattice of Propyl Radical (2). The results of the calculations are summarized in Table 2. The splitting caused by the direct $\pi-\pi$ interaction of SOMOs within a paramagnetic dimer is 0.203 eV, whereas the splittings caused by the other interactions are at least an order of magnitude smaller. The largest value is 0.013 eV, which is caused by the interactions of two molecules within a column (pathway 1, refer to Figure 12). There is no direct relationship between the energy splitting and the closest carbon−carbon contacts between phenalenyl units, indicating that the orientation and arrangement of the neighboring molecular pairs is the most important factor. Generally speaking, the phenalenyl units that are directly above each other have stronger interactions than those to the side of each other; and parallel planes interact much more strongly than those perpendicular to each other. This behavior may be attributed to the nodal properties of the pπ-orbitals that contain the spin density in the phenalenyl ring system.

Crystal Packing of the Hexyl Radical. The hexyl radical (**4**) does not form π-dimers, and is a much better conductor than the propyl radical (**2**); (σ_{RT} (**4**) $= 5.0 \times 10^{-2}$ S/cm and σ_{RT} (**2**) $= 1.4 \times 10^{-6}$ S/cm). There are eight molecules or four pairs of enantiomers in the unit cell of **4** (Figure 16). The four molecules along the top row of Figure 16 are of the same chirality, whereas the molecules on the bottom row are the corresponding enantiomers.

Each of these molecules forms columns along the *b* direction (Figure 17), and the interactions within all columns are identical. The closest carbon−carbon contact within each column has $d = 3.488$ Å, and the phenalenyl units involving this contact are perpendicular to each other, similar to those of propyl radical. This interaction is defined as "pathway 1".

In Figure 16, the interactions between molecules from neighboring columns are identified as follows: J and K, K and L, K and M, and L and N. Figure 18 shows the interactions

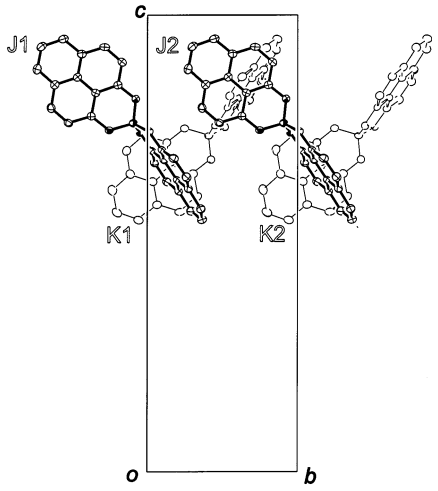

Figure 18. Molecule J interacts with K, and the combination of columns J and K forms a possible conducting pathway along the *b* direction.

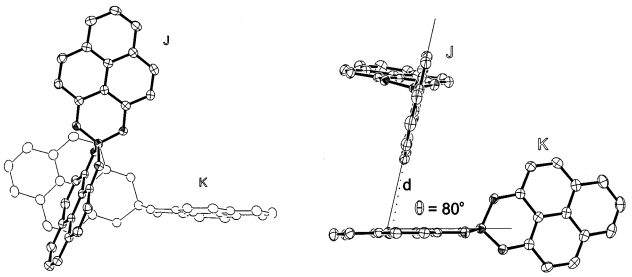

Figure 19. Phenalenyl units of molecule J and K are not perpendicular to each other, but lie at an angle of 80°, which allows for better overlap between the π-orbitals of the SOMOs of the phenalenyl units.

between columns J and K (view down *a*). If molecule J1 interacts with K1, K1 interact with J2, and J2 interacts with K2, a conducting pathway is possible along columns J and K, provided that this chain of interactions is viable.

The interaction between a pair of molecules from columns J and K is illustrated in Figure 19. Unlike the case of the propyl radical (**2**), the phenalenyl unit of J involved in the interaction in hexyl radical (**4**), is not perpendicular to that of K, but is inclined at an angle of 80°. This is the main point of differentiation between the packing of hexyl (**4**) and propyl (**2**) radicals, insofar as their conducting pathways are concerned, and we believe that it is this factor that is principally involved in determining their very different transport properties.

In crystals of propyl radical (**2**), all phenalenyl units are either perpendicular, or parallel to each other—if they are parallel, the phenalenyl units are always to the side of each other (except for the phenalenyl units involved in π-dimers). In the case of hexyl radical (**4**), the two phenalenyl units are not only directly above one another, but they are inclined away from a strictly perpendicular orientation. On the basis of the nodal characteristics of pure pπ-orbitals the deviation from a perpendicular orientation facilitates the overlap between the two SOMOs. While the closest carbon−carbon contact $d = 3.718$ Å is much greater than that within a column (pathway 1, $d = 3.488$ Å), the calculated splitting caused by J and K is 0.018 eV, more than twice the splitting calculated for pathway 1. This interaction between J and K is referred to as the interaction for "pathway 2".

The interactions between columns K and L are illustrated in Figure 20 (view down *a*). Although the phenalenyl units of L1 and K1 are far away from each other, molecule K1 can interact

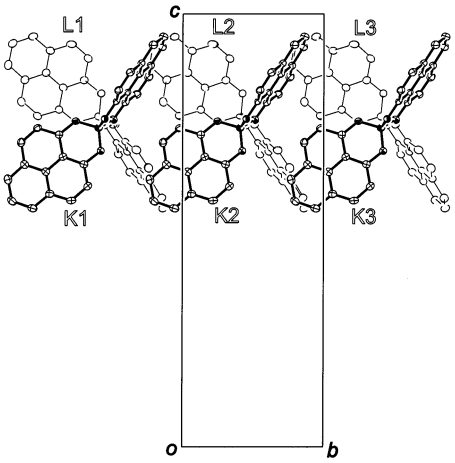

Figure 20. Columns of K and L interact with each other to form two separate conducting pathway, K1−L2−K3 and L1−K2−L3.

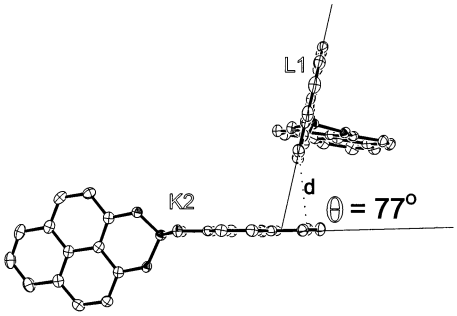

Figure 21. Interaction between L1 and K2.

with L2, and in turn L2 can interact with K3. Similarly L1−K2−L3 also interact, so that columns L and K interact with each other to form two separate and identical conducting pathways, providing that the interactions are significant.

The interaction between L1 and K2 is illustrated in Figure 21. Again the phenalenyl units are not perpendicular to each other, but have an angle of 77°, and the closest carbon−carbon contact is 3.688 Å. Because the angle is even smaller than that in "pathway 2", and the carbon−carbon contacts are comparable, the interaction between L1 and K2 is expected to be stronger than that between J and K (pathway 2). Indeed, the calculated splitting is 0.024 eV (defined as the interaction in "pathway 3"), the largest among the interactions found in crystalline hexyl radical (**4**).

Figure 22 illustrates the interactions between columns K and M, and L and N. The phenalenyl units of K and M are parallel to each other, and so are those of L and N. The closest carbon−carbon contacts are $d1 = 3.596$ Å and $d2 = 3.624$ Å, and these interaction are referred to as the interactions in "pathway 4" and "pathway 5", respectively. Since the splitting caused by L and N is very weak (Table 2), pathway 5 may be disregarded.

Columns K and M do not interact continuously along the b direction as do columns J and K (and also K and L). Nevertheless pathway 4 (interaction of K and M) is a viable route along the c direction, provided that the interaction between columns K and L is also included in the conducting pathway (Figure 23).

EHT Calculations on Pairs of Molecules in the Lattice of Hexyl Radical (4). The calculations on the hexyl radicals are summarized in the bottom half of Table 2. The largest splitting of the SOMOs is 0.024 eV, almost twice the highest value found in the propyl radical crystal (not including the intra-dimer interaction). This splitting is caused by the interaction of

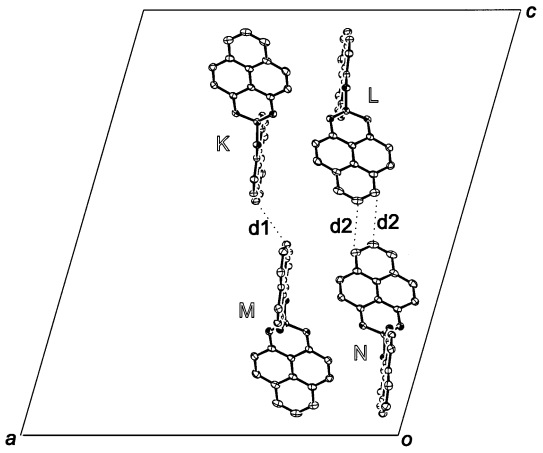

Figure 22. Interactions between columns of K and M, L, and N. The phenalenyl units of K and L are parallel to those of M and N, respectively.

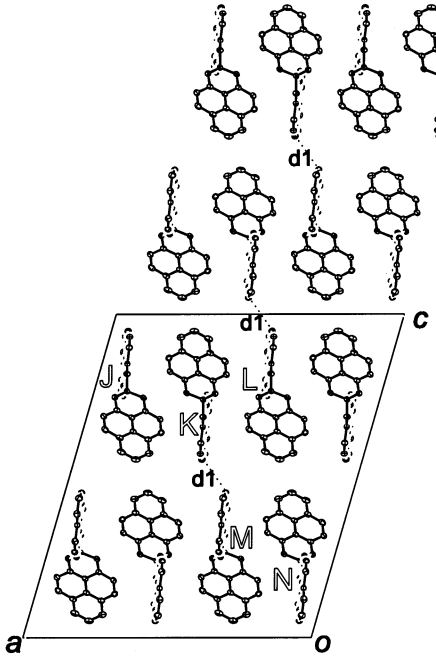

Figure 23. Pathway 4 along c involves a combination of interaction between K and M and that between K and L.

molecules in columns K and L. The nonperpendicular geometry of these phenalenyl units facilitates the overlap between the two π systems and the continuity provided by the interactions between these molecules forms an effective conducting pathway along the *b* direction. Indeed, the conductivity of the hexyl radical (**4**) is 4 orders of magnitude larger than that of propyl radical (σ_{RT} (**2**) $= 1.4 \times 10^{-6}$ S/cm), and reaches σ_{RT} (**4**) $= 5.0 \times 10^{-2}$ S/cm at room temperature, the highest so far among any neutral organic molecular solid.[7]

As noted above, the conductivities in a given direction are expected to scale approximately as the square of the transfer integrals, which are directly proportional to the energy splittings given in the Table. This relationship is valid within a particular compound, but because of the similarity of the molecules, it is natural to expect that it would be valid for comparisons drawn across all of the compounds. On the basis of the experimental conductivities of **2** and **4**, we would therefore expect a factor of 100 in the relative transfer integrals of the two compounds, and it is clear that the calculations cannot quantitatively account for the large difference in the relative effectiveness of conducting pathways in the two solids. This failure is surprising, given the success of such treatment with the organic superconductors such as $(TMTSF)_2X$,[12,23,35] and it is apparent that a full understanding of the conduction process in the neutral organic radicals remains to be established.

Finally, we note that although the present discussion has been couched in terms of the relative room-temperature conductivities of the radicals: $\sigma_{RT} = 1.0 \times 10^{-2}$ (**1**), 1.4×10^{-6} (**2**), 2.4×10^{-2} (**3**) and 4.9×10^{-2} (**4**) S/cm, or σ_{RT} (**1**):σ_{RT} (**2**):σ_{RT} (**3**):σ_{RT} (**4**) $=$ 0.2:0.000 03:0.5:1.0, exactly the same conclusions follow from the energy gaps (E_g) obtained by analyzing the temperature dependence of the conductivities of the paramagnetic radicals: $E_g = 0.12$ (**1**), 0.40 (**2**), 0.16 (**3**), 0.26 (**4**) eV.

Conducting Pathways in Organic Molecular Solids. The previous discussion has focused on the new phenalenyl-based neutral radical molecular conductors (**1**−**4**),[7,6] but we believe that our analysis has far reaching implications for conduction in organic molecular solids. The neutral radical molecular conductors are ideal systems for identifying viable conducting pathways for a number of reasons: (1) they are intrinsic semiconductors—most other neutral organic semiconductors depend on impurity doping for the generation of the carriers that lead to conductivity; (2) they have moderately high conductivities; (3) they do not suffer the complications that arise when counterions are present in the lattice; (4) the relevant intermolecular overlaps arise from molecular orbitals (SOMOs) that are composed of planar pπ-conjugated carbon atoms (the heterocyclic atoms are sterically shielded), and thus, the hybridization and directionality of the orbitals is not in doubt; (5) the spiro-linkage prevents stacking and their structures are not dictated by their open shell electronic structure; (6) the solids usually show paramagnetism over some temperature range and this property provides additional information on the electronic structure.

Our analysis supports previous work[16,20,30,31] that suggests that the interactions between neighboring organic molecules in the crystal lattice are dominated by their orientation and arrangement rather than by their interatomic separations (cf., Table 2). Heteroatoms are usually very efficient in facilitating intermolecular interactions[20,31,30,35] and their hybridizations sometimes introduce an additional degree of freedom in developing intermolecular overlap, but the present work shows that carbon−carbon interactions are surprisingly effective even when the interactions occur at distances that far exceed the sum of the van der Waals separations (3.4 Å)[16] and do not involve the type of head on π-orbital overlap that occurs in crystalline C_{60}, providing that the π-systems are not perpendicular. Relatively weak interactions between carbon-based pπ-systems (Table 2), are shown to be capable of supporting high conductivities that probably involve band transport[7] and the magnitude of the conductivity is exquisitely sensitive to the intermolecular overlaps and it seems likely that the EHT calculations are only partially successful in capturing the subtleties of these interactions. The conductivity process is largely decoupled from the magnetic properties − in the dimeric conductors ethyl (**1**) and butyl (**3**) the conductivity actually increases by 2 orders of magnitude as their structures change from paramagnetic to diamagnetic π-dimers.

Conclusion

We have undertaken a detailed analysis of the molecular packing of the propyl (**2**) and hexyl (**4**) radical crystals, and we are able to identify the features that are important in determining the viability of conducting pathways in organic molecular solids.

Interatomic separations alone are insufficient for such an analysis.

In crystals of propyl radical, all neighboring pairs of phenalenyl units are either perpendicular or parallel and offset. The $\pi-\pi$ interaction within a dimer leads to a large splitting of the SOMOs (0.203 eV), indicating that the interaction is strong. Since parallel phenalenyl units between dimers are to the side of each other, the splittings are general very small, indicating that these interactions are weak. For those phenalenyl units that are perpendicular to each other, even though they may be directly above each other and the carbon−carbon contact distances are quite small, the overlap between the two π systems is weak and the energy splitting is small; thus, the interaction between these phenalenyl units are also weak. Because the phenalenyl contacts in crystals of propyl radical are always confined to these two types, interactions between π-dimer pairs are too weak to form an effective conducting pathway.

In crystals of hexyl radical, there are also neighboring phenalenyl units perpendicular or parallel to (but offset from) each other. The calculations show these interactions are also as weak as in crystals of the propyl radical. However, there are also phenalenyl units in crystals of the hexyl radical that are not only above each other, but have angles of 75−80° between them. This geometry allows much better overlap between the π-orbitals of the phenalenyl units and is identified as the key factor in establishing a conducting pathway through the crystal. Moreover, these interactions are continuous along the *b* direction where the conductivity reaches 0.05 S/cm at room temperature, 4 orders of magnitude higher than that found in crystals of propyl radical.

Experimental Section

Materials. Boron trichloride (Aldrich) and cobaltocene (Strem) were all commercial products and were used as received. 9-hydroxyphenalenone and sodium tetrakis[3,5-bis(trifluoromethyl)phenyl]borate (sodium TFPB) were synthesized according to literature procedures.[21,19,1] Toluene was distilled from sodium benzophenone ketyl immediately before use. Acetonitrile was distilled from P_2O_5 and then redistilled from K_2CO_3 immediately before use. The heavy-walled glass tubes for high-pressure reactions are available form Ace Glass Inc., Vineland, NJ.

***N*-Propyl-9-amino-1-phenalenone.** A mixture of 9-hydroxyphenalenone (1.96 g, 0.01 mol) and propylamine (30 mL) was placed in a heavy-walled sealed tube with an Ace thread at one end and sealed with a Teflon plug. The contents were stirred at a temperature of 125 °C for 2 h. The mixture was allowed to cool, the tube vented, opened, and the contents poured into 100 mL distilled water. The aqueous mixture was extracted with CH_2Cl_2, the organic layer was separated, dried with potassium carbonate, and taken down on a rotary evaporator to give a brownish-yellow oil. The oil solidified overnight and was purified by column chromatography on alumina with chloroform. Crystallization from heptane gives yellow leafs. Yield: 1.51 g (60%); mp 60−61 °C. ^{1}H NMR (CD_3CN): δ 12.26 (b, 1H), 8.09 (d, 1H), 7.88−7.99 (m, 3H), 7.45 (t, 1H), 7.35 (d, 1H), 6.86 (d, 1H), 3.54 (d of t, 2H), 1.80 (t, 3H), 1.07 (t, 3H). Anal. Calcd for $C_{16}H_{15}ON$: C, 80.98; H, 6.37; N, 5.90. Found: C, 80.92; H, 6.48; N, 5.72.

Preparation of 2^+, Cl^-. *N*-Propyl-9-amino-1-phenalenone (1.3 g, 5.5 mmol) in anhydrous toluene (60 mL) was treated with boron trichloride in dichloromethane (2.6 mL, 2.6 mmol) under argon in the dark, and the mixture was refluxed for 20 h. The yellow solid was isolated by filtration (1.1 g, 79%). When a melting point determination was attempted, the salt turned black (∼150 °C). ^{1}H NMR (CD_3OD); δ 8.60 (d, 2H), 8.54 (d, 2H), 8.34−8.42 (m, 4H), 7.86 (t, 2H), 7.58 (d, 2H), 7.49 (d, 2H), 3.75 (b, 2H), 3.32 (b, 2H), 1.73−1.90 (m, 4H), 0.83 (t, 6H). IR (HART, 1700−690 cm^{-1}): 3029 (w), 2966 (w), 1626 (m), 1595 (w), 1585 (m), 1572 (m), 1514 (s), 1472 (w), 1448 (w), 1391 (m), 1354 (m), 1335 (w), 1291 (s), 1245 (m), 1198 (w), 1166 (w), 1135 (w), 1107 (w), 1021 (s), 974 (w), 911(w), 866 (m), 848 (m), 823 (w), 760 (m), 712 (w), 699 (w).

Preparation of 2^+, $TFPB^-$. A mixture of 2^+, Cl^- (0.5 g, 0.001 mole) and Na^+, $TFPB^-$ (0.9 g, 0.001 mole) was added to 40 mL of diethyl ether. The mixture was stirred for 15 min until all yellow solids went into the solution and a white solid had precipitated. The yellow solution was filtered through a D frit and the solvent was evaporated to give a brownish-yellow solid. Crystallization from benzene gave red cubes. Yield: 1 g (85%); mp 176−177.5 °C. ^{1}H NMR (CD_3CN): δ 8.53 (d, 2H), 8.45 (d, 2H), 8.29−8.37 (m, 4H), 7.82 (t, 2H), 7.62−7.72 (m, 12 H), 7.47 (d, 2H), 7.43 (d, 2H), 3.53−3.74 (b, 2H), 3.18−3.39 (b, 2H), 1.64−1.85 (m, 4H), 0.78 (t, 6H). IR (4000−400 cm^{-1}): ν = 2976 (w), 2945 (w), 2909 (w), 2884 (w), 1630 (m), 1587 (w), 1577 (m), 1518 (m), 1473 (w), 1390 (w), 1353 (m), 1294 (m), 1275 (s), 1244 (m), 1155 (m), 1122 (s), 1049 (w), 1035 (m), 1015 (m), 952 (w), 914 (w), 881 (m), 845 (m), 825 (w), 765 (w), 744 (w), 715 (m), 682 (m). Anal. Calcd for $C_{64}H_{40}O_2N_2B_2F_{24}$: C, 57.08; H, 2.99; N, 2.08; B, 1.61; F, 33.86. Found: C, 57.10; H, 2.99; N, 2.27; B, 1.54; F, 34.12.

Crystallization of 2. An invertable H-Cell with a glass D frit was loaded in a drybox. A solution of 150 mg (0.11 mmol) of 2^+, $TFPB^-$ in 12 mL dry CH_3CN was placed in one container, and 25 mg $CoCp_2$ (0.13 mmol) dissolved in 13 mL dry CH_3CN in the other container. The containers were attached to the inverted H-cell. The H-cell was removed from the drybox and attached to a vacuum line, and the containers taken through three cycles of freeze, pump and thaw to degas the solutions. The H-cell was inverted, and the solutions were allowed to diffuse through the glass frit. After sitting in the dark for one week the cell yielded 50 mg (80%) of black shining cubes. Anal. Calcd for $C_{32}H_{28}O_2N_2B$: C, 79.51; H, 5.84; N, 5.80; B, 2.24. Found: C, 79.34; H, 6.06; N, 5.94; B, 2.19.

X-ray Crystallography. Data were collected at ambient temperature by a Nonius CAD-4 system at University of Arkansas.

Magnetic Susceptibility Measurements. The magnetic susceptibility of **2** was measured over the temperature range of 5 to about 400 K on a George Associates Faraday balance operating at 0.5 T.

Conductivity Measurements. The single-crystal conductivity, σ, of **2** was measured in a four-probe configuration. The in-line contacts were made with silver paint. The samples were placed on a sapphire substrate and electrical connections between the silver paint contacts and substrate were made by thin, flexible 25 μm diameter silver wires to relieve mechanical stress during thermal cycling of the sample.

Conductivity was measured in a custom-made helium variable-temperature probe using a Lake Shore 340 temperature controller. A Keithley 236 unit was used as a voltage source and current meter, and two 6517A Keithley electrometers were used to measure the voltage drop between the potential leads in a four probe configuration.

EHT Calculations. The band structure calculations made use of a modified version of the extended Huckel theory (EHT) band structure program. The parameter set is chosen to provide a reasonably consistent picture of bonding in heterocyclic organic compounds.[9,20]

Acknowledgment. This work was supported by the Office of Basic Energy Sciences, Department of Energy, under Grant No. DE-FG03-01ER45879 and by Los Alamos National Laboratories, Grant No. STB-UC:10019-001.

References and Notes

(1) Bahr, S. R.; Boudjouk, P. *J. Org. Chem.* **1992**, *57*, 5545−5547.
(2) Bechgaard, K.; Carneiro, K.; Rasmussen, F. B.; Olsen, M.; Rindorf, G.; Jacobsen, C. S.; Pedersen, H. J.; Scott, J. C. *J. Am. Chem. Soc.* **1981**, *103*, 2440−2442.
(3) Bechgaard, K.; Cowan, D. O.; Bloch, A. N. *J. Chem. Soc., Chem. Commun.* **1974**, 937−938.
(4) Bender, K.; Hennig, I.; Schweitzer, D.; Dietz, K.; Endres, H.; Keller, H. J. *Mol. Cryst. Liq. Cryst.* **1984**, *108*, 359.
(5) Carlson, K. D.; Geiser, U.; Kini, A. M.; Wang, H. H.; Montgomery, L. K.; Kwok, W. K.; Beno, M. A.; Williams, J. M.; Cariss, C. S.; Crabtree, G. W.; Whangbo, M.-H.; Evain, M. *Inorg. Chem.* **1988**, *27*, 965.
(6) Chi, X.; Itkis, M. E.; Kirschbaum, K.; Pinkerton, A. A.; Oakley, R. T.; Cordes, A. W.; Haddon, R. C. *J. Am. Chem. Soc.* **2001**, *123*, 4041−4048.
(7) Chi, X.; Itkis, M. E.; Patrick, B. O.; Barclay, T. M.; Reed, R. W.; Oakley, R. T.; Cordes, A. W.; Haddon, R. C. *J. Am. Chem. Soc.* **1999**, *121*, 10 395−10 402.
(8) Coleman, L. B.; Cohen, M. J.; Sandman, D. J.; Yamagishi, F. G.; Garito, A. F.; Heeger, A. J. *Solid State Commun.* **1973**, *12*, 1125−1132.
(9) Cordes, A. W.; Haddon, R. C.; Oakley, R. T.; Schneemeyer, L. F.; Waszczak, J. V.; Young, K. M.; Zimmerman, N. M. *J. Am. Chem. Soc.* **1991**, *113*, 582.
(10) Ferraris, J.; Cowan, D. O.; Walatka, V.; Perlstein, J. H. *J. Am. Chem. Soc.* **1973**, *95*, 948−949.
(11) Garito, A. F.; Heeger, A. J. *Acc. Chem. Res.* **1974**, *7*, 232−240.
(12) Grant, P. M. *Phys. Rev. B* **1982**, *26*, 6888−6895.
(13) Haddon, R. C. *Nature* **1975**, *256*, 394−396.
(14) Haddon, R. C. *Aust. J. Chem.* **1975**, *28*, 2343−2351.
(15) Haddon, R. C. *Acc. Chem. Res.* **1992**, *25*, 127.
(16) Haddon, R. C.; Chi, X.; Itkis, M. E.; Anthony, J. E.; Eaton, D. L.; Siegrist, T. *J. Phys. Chem. B* **2002**, *106*, 8288−8292.
(17) Haddon, R. C.; Chichester, S. V.; Marshall, J. H. *Tetrahedron* **1986**, *42*, 6293−6300.
(18) Haddon, R. C.; Ramirez, A. P.; Glarum, S. H. *Adv. Mater.* **1994**, *6*, 316−322.
(19) Haddon, R. C.; Rayford, R.; Hirani, A. M. *J. Org. Chem.* **1981**, *46*, 4587.
(20) Haddon, R. C.; Siegrist, T.; Fleming, R. M.; Bridenbaugh, P. M.; Laudise, R. A. *J. Mater. Chem.* **1995**, *5*, 1719−1724.
(21) Haddon, R. C.; Wudl, F.; Kaplan, M. L.; Marshall, J. H.; Cais, R. E.; Bramwell, F. B. *J. Am. Chem. Soc.* **1978**, *100*, 7629−7633.
(22) Hofmann, R. *Solids and Surfaces*; VCH: New York, 1988.
(23) Ishiguro, T.; Yamaji, K.; Saito, G. *Organic Superconductors*, 2nd ed; Springer-Verlag: Berlin, 1998; Vol. 88.
(24) Kaminskii, V. F.; Prokhorova, T. G.; Shibaeva, R. P.; Yagubskii, E. B. *JEPT Lett.* **1984**, *39*, 17−20.
(25) Kini, A. M.; Geiser, U.; Wang, H. H.; Carlson, K. D.; Williams, J. M.; Kwok, W. K.; Vandervoort, K. G.; Thompson, J. E.; Stupka, D. L.; Jung, D.; Whangbo, M.-H. *Inorg. Chem.* **1990**, *29*, 2555−2557.
(26) Kistenmacher, T. J.; Phillips, T. E.; Cowan, D. O. *Acta Crystallogr.* **1974**, *B30*, 768.
(27) Parkin, S. S. P.; Engler, E. M.; Schumaker, R. R.; Lagier, R.; Lee, V. Y.; Scott, J. C.; Greene, R. L. *Phys. Rev. Lett.* **1983**, *50*, 270−273.
(28) Phillips, T. E.; Kistenmacher, T. J.; Ferraris, J. P.; Cowan, D. O. *Chem. Commun.* **1973**, 471−473.
(29) Schoen, J. H.; Kloc, C.; Batlogg, B. *Phys. Rev. Lett.* **2001**, *86*, 3843.
(30) Siegrist, T.; Fleming, R. M.; Haddon, R. C.; Laudise, R. A.; Lovinger, A. J.; Katz, H. E.; Bridenbaugh, P.; Davis, D. D. *J. Mater. Res.* **1995**, *10*, 2170−2173.
(31) Siegrist, T.; Kloc, C.; Laudise, R. A.; Katz, H. E.; Haddon, R. C. *Adv. Mater.* **1998**, *10*, 379−382.
(32) Torrance, J. B. *Acc. Chem. Res.* **1979**, *12*, 79−86.
(33) Urayama, H.; Yamochi, H.; Saito, G.; Sato, S.; Kawamoto, A.; Tanaka, J.; Mori, T.; Maruyama, Y. *Chem. Lett.* **1988**, 463.
(34) Williams, J. M.; Emge, T. J.; Wang, H. H.; Beno, M. A.; Copps, P. T.; Hall, L. N.; Carlson, K. D.; Crabtree, G. W. *Inorg. Chem.* **1984**, *23*, 2558.
(35) Williams, J. M.; Ferraro, J. R.; Thorn, R. J.; Carlson, K. D.; Geiser, U.; Wang, H. H.; Kini, A. M.; Whangbo, M.-H. *Organic Superconductors (Including Fullerenes)*; Prentice Hall: Englewood Cliffs, NJ, 1992.
(36) Wudl, F.; Smith, G. M.; Hufnagel, E. J. *Chem. Commun.* **1970**, 1453−1454.
(37) Yagubskii, E. B.; Shchegolev, I. F.; Laukhin, V. N.; Kononovich, P. A.; Karatsovnik, M. V.; Zvarykina, A. V.; Buravov, L. I. *JETP Lett.* **1984**, *39*, 12−16.
(38) Yamochi, H.; Komatsu, T.; Matsukawa, N.; Saito, G.; Mori, T.; Kusunoki, M.; Sakaguchi, K. *J. Am. Chem. Soc.* **1993**, *115*, 11 319.